Fibrotic matrix induces mesenchymal transformation of epithelial cells in oral submucous fibrosis

Kai Jiao (kjiao1@163.com)
School of Stomatology, The Fourth Military Medical University, Xi'an, Shaanxi 710032, China.
Hao-qing Xu
1 Northwest University 2 The Fourth Military Medical University
Zhen-xing Guo
The Fourth Military Medical University
Jia-lu Gao
The Fourth Military Medical University
Shu-yan Wang
The Fourth Military Medical University
Jian-fei Yan
The Fourth Military Medical University
Xiao-xiao Han
1 Northwest University 2 The Fourth Military Medical University
Wen-pin Qin
The Fourth Military Medical University
Weicheng Lu
The Third Affiliated Hospital of Air Force Medical University
Chang-he Gao
The Third Affiliated Hospital of Xinxiang Medical University
Li-na Niu
The Fourth Military Medical University https://orcid.org/0000-0002-6653-0819

Article

Keywords: Oral submucous fibrosis, Malignant transformation, epithelial cells, Collagen matrix, Epithelial mesenchymal transformation

Posted Date: November 17th, 2022

DOI: https://doi.org/10.21203/rs.3.rs-2239264/v1

Abstract

Oral submucous fibrosis (OSF) is a precancerous state of the oral mucosa; however, whether and how the fibrotic matrix of OSF is involved in the malignant transformation of epithelial cells remains unknown. Herein, oral mucosa tissue from patients with OSF, arecoline-induced rat OSF models, and their controls were used to observe the extracellular matrix changes and epithelial-mesenchymal transformation (EMT) in fibrotic lesions, and to explore the effects and mechanism of matrix stiffness on epithelial cell EMT. Compared with the controls, oral mucous tissues from patient exhibited increased number of myofibroblasts, decreased number of blood vessels and increased type I and type III collagen levels, with thicker, less porous, and disorderly arranged fibers. The oral mucous tissues from humans and OSF rats showed increased stiffness compared with the controls, accompanied by increased EMT activities of epithelial cells. Moreover, stiff collagen constructs caused increased EMT and proliferation of epithelial cells compared with soft constructs, and caused increased expression of Piezo1 and YAP. The EMT activities of stiff construct-cultured epithelial cells were significantly increased by exogenous Piezo1 activation, and decreased by YAP inhibition. During *ex vivo* implantation, the cells in the epithelium of the stiff group showed increased EMT activities and increased levels of Piezo1 and YAP compared with those in the sham and soft groups. We concluded that increased stiffness of the fibrotic matrix in OSF led to increased proliferation and EMT of mucosal epithelial cells, in which the Piezo1-YAP signal transduction is important.

1. Introduction

Oral submucous fibrosis (OSF) is defined as a chronic progressive oral mucosal disease that is closely related to betel nut chewing.[1,2] OSF can occur in multiple parts of the patient's mouth, including the buccal mucosa, labial mucosa, molar pad, soft palate, and the bottom of the mouth, resulting in loss of fiber elasticity and increased mucosal stiffness.[3] The main clinical symptom of OSF is progressive mouth opening limitation, which affects chewing, swallowing, pronunciation, and other functions, which significant affects the quality of a patients' life.[4] As early as 1978, the World Health Organization (WHO) classified OSF as a precancerous state of the oral mucosa, which is closely related to the occurrence and development of oral squamous cell carcinoma.[3,5] Many epidemiological studies have shown that the canceration rate of OSF has reached 7.6–13%.[4,6] However, the specific mechanism of the development of cancer from OSF remains poorly understood and needs further exploration.

Fibrosis can occur in many different organs of the body and is a very important risk factor for cancer occurence.[7–9] For example, it has been reported that the incidence of lung cancer is markedly increased in patients with pulmonary fibrosis,[8] and the primary alveolar epithelial cells from the fibrotic lung exhibited enhanced cell migration and undergo epithelial-mesenchymal transformation (EMT), a mechanism that is closely related to cancer development.[10–12] Moreover, when the liver disease is out of control, progressive tissue fibrosis will eventually lead to cirrhosis and even malignant change. The expression levels of invasion and metastasis-related genes of hepatocellular carcinoma (HCC) were

significantly increased in a high-stiffness matrix compared with those in the controls.[13] Furthermore, high matrix stiffness is sufficient to drive EMT of HCC cells, which is consistent with the results of breast cancer cells.[14] The above studies showed that increased stiffness of the extracellular matrix (ECM) could induce EMT of diseased epithelial cells; however, the mechanism by which the cells perceive the physical changes to the ECM, especially during the development of OSF, remains unclear.

Piezo-type mechanosensitive ion channel component 1 (Piezo1) is widely expressed in non-sensory cells and serves as a key sensor of mechanical stimuli.[15–17] The morphology and migration activities of human epidermal keratinocytes in response to mechanical stimulus are affected by Piezo1 regulation.[18] Notably, oral mucosal cells express Piezo1, which is related to the activation of the yes-associated protein (YAP) signaling pathway.[19] Moreover, recent studies have shown that Piezo1 could act upstream of YAP in the differentiation of human neural stem cells and the development of zebrafish heart.[20,21] Therefore, we hypothesized that the ECM with increased stiffness in OSF mediates the EMT process of epithelial cells through the Piezo1/YAP signaling pathway.

To verify our hypothesis, oral mucosa tissue from patients with OSF, arecoline induced rat OSF models, and their controls were collected for histopathological, microstructural, and mechanical analysis to observe the changes in the ECM and EMT in fibrotic lesions. Then, the effects and mechanism of matrix stiffness on EMT were explored by culturing cells on collagen matrices with different degrees of stiffness in vitro. Furthermore, implanting these collagen matrices under the oral mucosa of rats was used to further confirm whether the stiffness of the ECM triggers EMT *ex vivo*.

2. Results And Discussion

Samples of human OSF and normal oral mucosa were collected to study the pathological characteristics of OSF. After histological staining of the tissue sections, we observed that the epithelial ridges of the fibrotic oral mucosa were reduced, and the collagen in the connective tissue area was significantly increased and denser (Fig. 1a-c). Immunohistochemical staining found that the number of alpha smooth muscle actin (α-SMA)-positive myofibroblasts in the connective tissue was increased, the number of CD31 (also known as PECAM1, platelet and endothelial cell adhesion molecule 1)-positive blood vessels in the tissue were reduced and became occluded (Fig. 1d-f), which were consistent with the characteristics of OSF.[22–24] In addition, Sirius red staining and micro-infrared analysis were used to compare the collagen characteristics of OSF and normal mucosa tissues. According to the collagen color under polarized light[25,26] and the change of collagen absorption peak,[27] type I and type III collagen levels in the fibrotic mucosa tissue were increased, which is consistent with previous results reported for OSF tissues (Fig. 1g-k).[28,29] The above results indicated that the number of myofibroblasts in OSF tissue increases and the cells secrete more collagen, which accumulates in the tissue, resulting in significant changes in the ECM collagen content.

Scanning electron microscopy (SEM) was used to further study the structural changes of the fibrotic oral mucosa. The results showed that the porosity of collagen in the connective tissue of OSF decreased, the transverse structure of some collagen disappeared, and collagen was denatured (Fig. 2a, b). Atomic force microscopy (AFM) was then used to evaluate the microscopic morphology and nano-mechanical properties of the oral mucosa connective tissue. We observed that the collagen was thick and disordered. Young's modulus analysis showed that the stiffness of OSF tissue was increased (Fig. 2c, d), which was consistent with previous results.[30] These results showed that the OSF tissue became stiffer because of the changes in collagen components, structure, and morphology. Previous studies showed that high stiffness of the ECM was related to the EMT of tissue cells;[31–33] therefore, we further detected the protein expression of EMT markers in OSF tissue using immunohistochemical staining. The results showed that the level of E-cadherin in epithelial cells of OSF tissue was decreased compared with that of the normal tissue, while the level of vimentin, a fibroblast marker, increased in the epithelial cells of OSF tissue (Fig. 2e-g), which is consistent with the characteristics of EMT.[34] The above findings indicated that the increased stiffness of OSF tissue was accompanied by increased EMT in the OSF tissue, suggesting that the EMT changes of epithelial cells in the OSF tissue might be mediated by the changes to extracellular collagen, resulting in increased tissue stiffness.

Next, we constructed a rat model of OSF by smearing and injecting arecoline into the oral mucosa of rats for 10 weeks.[35,36] Histological staining showed decreased epithelial ridges and increased collagen contents in the connective tissue of rat OSF samples compared with those in the controls (Fig. 3a, b). Similar to the results for human OSF samples, type I and type III collagen levels increased (Fig. 3c-g), the collagen became thicker and disordered, and tissue stiffness increased in the rat OSF samples compared with those in the controls (Fig. 3h-k). In addition, the level of Ecadherin in epithelial cells was reduced in the rat OSF samples compared with that in the controls (Fig. 3l, m), which was consistent with the characteristics of EMT and the results for the human OSF samples. However, the levels of vimentin did not differ significantly between the rat OSF samples and the controls, which might be related to the different pathological process of the rat model of OSF. The present rat model of OSF exhibited changes consistent with the middle to late stages of OSF, in which the whole process of EMT may not be complete. [37, 38]

To further verify the influence of the mechanical properties of the ECM on EMT, we used collagen constructs at 5 mg/ml and 35 mg/ml to simulate the soft and stiff ECM (Fig. 4a). Infrared spectrum analysis showed that the collagen in solution successfully self-assembled into collagen protein constructs with a complete structure *in vitro* (Fig. 4b). AFM was used to analyze the microscopic morphology and mechanical properties of the collagen constructs (Fig. 4c, d). The Young's modulus of the 35 mg/ml collagen construct (stiff construct) was significantly higher than that of the 5mg/ml collagen construct (soft constructs), and the porosity of the stiff construct was decreased significantly (Fig. 4e, f). Subsequently, the proliferation, morphology, and EMT on soft and stiff collagen constructs were investigated.

Cell Counting Kit 8 (CCK8) assays showed that the proliferation of epithelial cells on the stiff constructs was significantly higher than that on the soft constructs (Fig. 5a). The proliferation activities of epithelial cells were further evaluated by immunofluorescent staining of Ki67 and quantitative real-time polymerase chain reaction analysis of Cyclin E. The results showed that the protein level of Ki67 and mRNA expression of Cyclin E both increased in stiff construct group comparing to those in the soft construct group, in accordance to the results of CCK8 (Fig. 5b, c). The cells cultured on the soft matrix were irregular polygons, while the cells cultured on the stiff matrix were spindle shaped (Fig. 5d), similar to fibroblasts.[39] In addition, the mRNA and protein expression levels of E-cadherin decreased and those of vimentin increased in the stiff constructs group compared with those in the soft group (Fig. 5e-g), indicating that EMT occurred in epithelial cells cultured on the stiff collagen constructs.

However, how does the mechanical force of ECM affect the malignant transformation of cells? Previous studies have shown that Piezo1 can sense the mechanical changes of the ECM, thus opening the ion channel and mediating changes to the cell.[40,41] YAP is a key molecule of mechanical transduction, which can respond to the mechanical changes of the cell and enter the nucleus to regulate the expression of a variety of genes related to cancer.[42–44] Therefore, we detected these two proteins in epithelial cells, and found that their levels were increased in cells cultured on the stiff matrix, and YAP showed obvious nuclear translocation (Fig. 6a-c). These results confirmed that a stiff ECM can cause EMT in epithelial cells and that this change is related to the increased expression of Piezo1 and YAP.

To further verify the role of Piezo1 and YAP in EMT in response to a stiff matrix, we used the Piezo1 activator Yoda1 ((2-[5-[[(2,6-Dichlorophenyl)methyl]thio]-1,3,4-thiadiazol-2-yl]-pyrazine) to treat the cells growing on the stiff matrix. Activation of Piezo1 increased the mRNA and protein expression levels of YAP and vimentin, enhanced the nuclear translocation of YAP, and further decreased mRNA and protein expression levels of E-cadherin (Fig. 6d-f). This indicated that Piezo1 might mediate epithelial cell EMT through YAP. Next, epithelial cells cultured on the stiff matrix were treated with the YAP inhibitor Verteporfin. In response, the mRNA and protein expression levels of Piezo1 did not change significantly; however, the mRNA and protein expression levels of E-cadherin increased and those of vimentin decreased (Fig. 6g-i). The EMT of the cells was also inhibited. This indicated that YAP plays a key role in the cell phenotypic changes caused by EMT, and Piezo1 might function upstream of YAP to sense the extracellular mechanical changes, thus mediating EMT in response to the mechanical stimulus from a stiff matrix.

Next, we implanted the soft and stiff collagen constructs into the oral mucosa of rats to verify the above results (Fig. 7a). The results showed that in the stiff collagen implantation group, the cells within the epithelium expressed increased levels of vimentin, Piezo1, and YAP, but decreased levels of E-cadherin, compared with those in the epithelial cells in the sham control and the soft collagen implantation groups (Fig. 7b, c). The levels of vimentin, E-cadherin, Piezo1, and YAP in epithelial cells did not exhibit significant differences between the soft collagen implantation group and sham control group (Fig. 7b, c).

In this study, we found that the stiff OSF matrix can induce EMT, in which Piezo1 and YAP play key roles for signal transduction. Specifically, with the increased stiffness of the oral mucosa during OSF progression, Piezo1 senses the mechanical changes of the mucous matrix and induces YAP to undergo nuclear translocation, promoting the transcription and expression of EMT-related genes (e.g., *SNAI1*, *MMP9*, *QSOX1*, and *ZEB1*)[45,46], ultimately causing the cells to undergo EMT (Fig. 8). Therefore, local injection of enzymes related to collagen degradation or cross-linking to reverse the stiff characteristics of the fibrotic matrix might help to prevent the malignant transformation of epithelial cells in OSF.[47–49]

3. Conclusions

The present study demonstrated that the increased stiffness of the fibrotic matrix in OSF leads to increased proliferation and EMT of mucosal epithelial cells, in which the Piezo1-YAP axis plays important roles during mechanical sensing and signal transduction. Strategies to reverse the stiff fibrotic matrix are important to prevent EMT changes of mucosal epithelial cells in OSF.

4. Materials And Methods

4.1 Human oral mucosa specimens

Fibrous oral mucosa samples were obtained from patients with OSF lesions who were diagnosed by the Pathology Department of The Fourth Military Medical University. Normal human oral mucosa was obtained from patients with mucosal hyperplasia requiring tissue resection. All specimens were obtained with informed consent and authorization from the ethical committee of the Fourth Military Medical University (IRB-REV-2022058).

4.1.1 Histological and immunohistochemical staining

Specimens were fixed in 4% paraformaldehyde, dehydrated in an ascending ethanol series, embedded in paraffin, deparaffinized, and rehydrated in xylene and a descending series of ethanol. According to the supplier's instructions, hematoxylin and eosin, Masson tricolor, Sirius red, and immunohistochemical staining of 5 μm thick sections (n = 6) were performed, followed by observation under an optical microscope and a polarized light microscope. Digitized images of the stained sections were analyzed using ImageJ software (NIH, Bethesda, MN, USA).

4.1.2 Micro-Fourier Transform Infrared Spectroscopy (μ-FTIR)

The spotlight 400 m-FTIR imaging system (PerkinElmer, Inc., Waltham, MA, USA) was used to analyze the paraffin sections naturally dried after hydration. The resolution of spectral acquisition was 4 cm^{-1}, ranging from 650 to 4000 cm^{-1}, and 36 scans were used for each sample. Spectrum software (PerkinElmer, Inc.) was used to obtain the absorption wavelengths.

4.1.3 Scanning electron microscopy (SEM)

Fresh mucosa was fixed with 2.5% glutaraldehyde and dehydrated using an ascending ethanol series (30%, 50%, 70%, 80%, 90%, and 100% ethanol). Then, the sample was covered with hexamethyldisilazane and air dried slowly. Finally, it was sputtered with gold and examined using a field emission scanning electron microscope (FE-SEM, S-4800, Hitachi, Tokyo, Japan) at 5 kV. ImageJ software was used to analyze the SEM images.

4.1.4 Atomic force microscopic (AFM)

AFM (Keysight 5500, Keysight Technologies, Santa Rosa, CA, USA) was used to analyze 10 μm paraffin sections. After the hydrated sections were naturally dried, a silicon probe (PPP-NCLR-20, Nanosensors™, Neuchatel, Switzerland) with a force constant of 42 N/m and a resonance frequency of 161 kHz was used to perform micromorphological imaging of the oral mucosa connective tissue. The hydrated slice was immersed in normal saline at room temperature and a silicon oxide tip (SD-Sphere-CONT-m-10, Nanosensors™) with a force constant of 0.2 N/m and resonance frequency of 13 kHz was used to perform mechanical tests on the oral mucosa connective tissue, measuring the elastic modulus of each position at an indentation depth of 300 nm. All measurements were repeated for six locations of each tissue sample and the average was taken.

4.2 OSF rat model establishment

Male Sprague-Dawley rats were obtained from the Experimental Animal Research Center of the Fourth Military Medical University. The animal experiments were conducted in accordance with the guidelines formulated by the Animal Research Committee of the School of Stomatology of the Fourth Military Medical University, and were approved by the committee.

Arecoline (SA9640, Solarbio, Beijing, China, 10 mg/mL and 5 mg/mL) was dissolved in 0.9% normal saline, and the animal model was established by oral smearing and submucosal injection. The frequency of smearing application was once a day. The injection frequency was once every three days, and the injection volume of arecoline solution was 50 μL. After arecoline treatment, no food or water was provided for 2 hours. After 10 weeks of arecoline intervention, the rat model of OSF was established, all animals were killed, and their oral mucosa tissues were collected for subsequent analysis.

4.3 Construction of collagen matrix

A rat tail was immersed in 75% alcohol for 30 minutes to peel off the skin. The tip of the tail was clamped with tweezers to extract the collagen. After washing, the rat tail was immersed in Tris-HCl and NaCl mixture at 4 ℃ overnight. The collagen was taken out and dissolved in 0.3 M acetic acid solution. After centrifugation, the collagen solution was placed in a dialysis bag (MD25 (8000–14000 Da)) and dialyzed in phosphate-buffered saline (PBS) until the pH of the PBS remained at 7. At this time, the solid collagen block was taken and stored at 4 ℃ in 75% alcohol. Before use, the collagen block was frozen and cut into 2–4 mm thick pieces.

4.4 Cell culture

A human oral epithelial cell (HOK, HUM-iCELL-m004, China) was used. The cut collagen pieces were placed in the wells of a 24-well plates, washed PBS many times, and then the cells were inoculated onto the collagen matrix. All cells were cultured in Dulbecco's modified Eagle's medium high glucose medium at 37°C and 5% CO_2.

4.4.1 Cell proliferation test

Cells were inoculated into 96-well plates (5000 cells/well). After 24, 48, and 72 hours of culture, cell proliferation was evaluated using Cell Count Kit-8 analysis (CCK-8, Dojindo, Japan) according to the manufacturer's instructions. A microplate reader (BioTek, Winooski, VT, USA) was used to measure the absorbance value at 450 nm.

4.4.2 Signal activation and inhibition

The Piezo1 activator Yoda1 (HY-18723, Med Chem Express, America) and the YAP inhibitor Verteporfin (HY-B0146, Med Chem Express, America) were respectively dissolved in DMSO according to the manufacture instructions, and added into the cell culture medium. The working concentration of Yoda1 and Verteporfin were 300nM and 3μM according to previous studies.[50,51]

4.4.3 Immunofluorescence

The culture medium was discarded, the cells were washed using PBS three times, 4% paraformaldehyde was added to fix the cells for 10 minutes, the cells were washed using PBS three times, 0.1% triton was added to treat the cells for 10 minutes, the cells were washed again, serum was incubated with the cells to block them for 30 minutes, and then the cells were exposed to the primary antibodies at 4°C overnight. The antibodies used were Piezo1 (1:300, DF12083, Affinity), YAP (1:300, 66900-1-lg, Proteintech), E-cadherin (1:300, AF0131, Affinity), Vimentin (1:300, 10366-1-AP, Proteintech) and Ki67 (1:300, AF0198, Affinity). After PBS washing, the secondary antibody was added and incubated for 1 h in the dark. The processed cells were mounted in Antifade Mountant with 4',6-diamidino-2-phenylindole (DAPI; Invitrogen, Waltham, MA, USA) for confocal scanning laser microscopy (CLSM) (Nikon A1R, Nikon Corporation, Minato-ku, Tokyo, Japan) according to the manufacturer's instructions. The integrated fluorescence intensity was calculated using the ImageJ software.

4.4.4 Quantitative reverse transcription-polymerase chain reaction (qRT-PCR)

Total RNA was extracted from the human oral epithelial cell using the Trizol reagent (Invitrogen). The concentration and purity of the extracted RNA were determined by measuring the absorbance at 260 and 280 nm (BioTek). cDNA was synthesized using a PrimeScript RT reagent kit (Takara Bio Inc., Shiga, Japan) and quantitative real-time PCR (7500 Real-time PCR System; Applied Biosystems, Carlsbad, CA, USA) was performed. *GAPDH* (encoding glyceraldehyde-3-phosphate dehydrogenase) was used as the

housekeeping gene. Fold changes relative to the control group were estimated using the $2^{-\Delta\Delta Ct}$ method.[52] The primer sequences are presented in Supplementary Table 1.

4.5 Subcutaneous collagen implantation

Incisions were made in the oral mucosa of the rats, the collagen block was placed under the mucosa, and then the tissue incisions were sutured. Seven days later, the rats were killed to take samples.

4.6 Statistical analyses

All data are expressed as the mean ± standard deviation. The Shapiro–Wilk test was used to test the normal distribution (95% confidence interval). Levene's test was used to evaluate the homogeneity of variance. A T test was used to compare the differences between the two groups. Univariate and bivariate analysis of variance (ANOVA) were used to assess the differences between groups. The GraphPad Prism 8 software package (GraphPad Software, La Jolla, CA, USA) was used for analysis. Significance was accepted when $p < 0.05$.

Declarations

Acknowledgments

This work was supported by grants 82170978 from National Natural Science Foundation of China, grant 2021JC-34 from the Distinguished Young Scientists Funds of Shaanxi Province, and grant 2020TD-033 from the Shaanxi Key Scientific and Technological Innovation Team.

Conflict of interests

The author denies any competitive conflict of interest or personal relationship that may affect the work covered in this article.

Author Contributions

Kai Jiao and Li-na Niu revised the manuscript, supervised the project and provided financial support. Hao-qing Xu, Zhen-xing Guo, Jia-lu Gao and Shu-yan Wang conducted experiments and analyzed the data. Jia-lu Gao and Hao-qing Xu participated in drawing the schematic diagram of the article. Hao-qing Xu and Zhen-xing Guo drafted the primary manuscript. Jian-fei Yan, Xiao-xiao Han, Wen-pin Qin, Wei-cheng Lu and Chang-he Gao contributed to the writing of manuscript and analyzed the data. Hao-qing Xu and Zhen-xing Guo contributed equally to this paper.

References

1. Binnal A, Tadakamadla J, Rajesh G, Tadakamadla SK. Photodynamic therapy for oral potentially malignant disorders: A systematic review and meta-analysis. *Photodiagnosis Photodyn Ther* **37**, 102713 (2022)

2. Li J, Yao M, Zhu X, Li Q, He J, Chen L, et al. YAP-Induced Endothelial-Mesenchymal Transition in Oral Submucous Fibrosis. *J Dent Res* **98**, 920-929 (2019)
3. Mahomed F. Oral submucous fibrosis--a potentially malignant condition of growing concern. *SADJ* **67**, 562, 564-565 (2012)
4. Lin HJ, Lin JC. Treatment of oral submucous fibrosis by collagenase: effects on oral opening and eating function. *Oral Dis* **13**, 407-413 (2007)
5. Warnakulasuriya S, Kujan O, Aguirre-Urizar JM, Bagan JV, Gonzalez-Moles MA, Kerr AR, et al. Oral potentially malignant disorders: A consensus report from an international seminar on nomenclature and classification, convened by the WHO Collaborating Centre for Oral Cancer. *Oral Dis* **27**, 1862-1880 (2021)
6. You Y, Huang Y, Wang D, Li Y, Wang G, Jin S, et al. Angiotensin (1-7) inhibits arecoline-induced migration and collagen synthesis in human oral myofibroblasts via inhibiting NLRP3 inflammasome activation. *J Cell Physiol* **234**, 4668-4680 (2019)
7. Baglieri J, Brenner DA, Kisseleva T. The Role of Fibrosis and Liver-Associated Fibroblasts in the Pathogenesis of Hepatocellular Carcinoma. *Int J Mol Sci* **20**, 1723 (2019)
8. Kinoshita T, Goto T. Molecular Mechanisms of Pulmonary Fibrogenesis and Its Progression to Lung Cancer: A Review. *Int J Mol Sci* **20**, 1461 (2019)
9. Konigshoff M. Lung cancer in pulmonary fibrosis: tales of epithelial cell plasticity. *Respiration* **81**, 353-358 (2011)
10. Konigshoff M, Kramer M, Balsara N, Wilhelm J, Amarie OV, Jahn A, et al. WNT1-inducible signaling protein-1 mediates pulmonary fibrosis in mice and is upregulated in humans with idiopathic pulmonary fibrosis. *J Clin Invest* **119**, 772-787 (2009)
11. Willis BC, Liebler JM, Luby-Phelps K, Nicholson AG, Crandall ED, du Bois RM, et al. Induction of epithelial-mesenchymal transition in alveolar epithelial cells by transforming growth factor-beta1: potential role in idiopathic pulmonary fibrosis. *Am J Pathol* **166**, 1321-1332 (2005)
12. Kim KK, Kugler MC, Wolters PJ, Robillard L, Galvez MG, Brumwell AN, et al. Alveolar epithelial cell mesenchymal transition develops in vivo during pulmonary fibrosis and is regulated by the extracellular matrix. *Proc Natl Acad Sci U S A* **103**, 13180-13185 (2006)
13. Dong YY, Zheng QD, Wang ZM, Lin XH, You Y, Wu SF, et al. Higher matrix stiffness as an independent initiator triggers epithelial-mesenchymal transition and facilitates HCC metastasis. *J Hematol Oncol* **12**, 112 (2019)
14. Wei SC, Fattet L, Tsai JH, Guo YR, Pai VH, Majeski HE, et al. Matrix stiffness drives epithelial mesenchymal transition and tumour metastasis through a TWIST1-G3BP2 mechanotransduction pathway. *Nat Cell Biol* **17**, 678-U306 (2015)
15. Li J, Hou B, Tumova S, Muraki K, Bruns A, Ludlow MJ, et al. Piezo1 integration of vascular architecture with physiological force. *Nature* **515**, 279-282 (2014)
16. Yang XN, Lu YP, Liu JJ, Huang JK, Liu YP, Xiao CX, et al. Piezo1 Is as a Novel Trefoil Factor Family 1 Binding Protein that Promotes Gastric Cancer Cell Mobility In Vitro. *Digest Dis Sci* **59**, 1428-1435

(2014)

17. Yu JL, Liao HY. Piezo-type mechanosensitive ion channel component 1 (Piezo1) in human cancer. *Biomed Pharmacother* **140**, 111692 (2021)
18. He JH, Shan SZ, Li QF, Fang B, Xie Y. Mechanical Stretch Triggers Epithelial-Mesenchymal Transition in Keratinocytes Through Piezo1 Channel. *Front Physiol* **13**, 745572 (2022)
19. Hasegawa K, Fujii S, Matsumoto S, Tajiri Y, Kikuchi A, Kiyoshima T. YAP signaling induces PIEZO1 to promote oral squamous cell carcinoma cell proliferation. *J Pathol* **253**, 80-93 (2021)
20. Pathak MM, Nourse JL, Tran T, Hwe J, Arulmoli J, Le DT, et al. Stretch-activated ion channel Piezo1 directs lineage choice in human neural stem cells. *Proc Natl Acad Sci U S A* **111**, 16148-16153 (2014)
21. Duchemin AL, Vignes H, Vermot J. Mechanically activated piezo channels modulate outflow tract valve development through the Yap1 and Klf2-Notch signaling axis. *Elife* **8**, e44706 (2019)
22. Das RK, Anura A, Pal M, Bag S, Majumdar S, Barui A, et al. Epithelio-mesenchymal transitional attributes in oral sub-mucous fibrosis. *Exp Mol Pathol* **95**, 259-269 (2013)
23. Gupta K, Metgud R, Gupta J. Evaluation of stromal myofibroblasts in oral leukoplakia, oral submucous fibrosis, and oral squamous cell carcinoma–an immunohistochemical study. *J Cancer Res Ther* **11**, 893-898 (2015)
24. Sharma E, Tyagi N, Gupta V, Narwal A, Vij H, Lakhnotra D. Role of angiogenesis in oral submucous fibrosis using vascular endothelial growth factor and CD34: An immunohistochemical study. *Indian J Dent Res* **30**, 755-762 (2019)
25. Brown SR, Cleveland EM, Deeken CR, Huitron SS, Aluka KJ, Davis KG. Type I/type III collagen ratio associated with diverticulitis of the colon in young patients. *J Surg Res* **207**, 229-234 (2017)
26. Wang L, Hu L, Zhou X, Xiong Z, Zhang C, Shehada HMA, et al. Exosomes secreted by human adipose mesenchymal stem cells promote scarless cutaneous repair by regulating extracellular matrix remodelling. *Sci Rep* **7**, 13321 (2017)
27. Belbachir K, Noreen R, Gouspillou G, Petibois C. Collagen types analysis and differentiation by FTIR spectroscopy. *Analytical and bioanalytical chemistry* **395**, 829-837 (2009)
28. Zhang SS, Gong ZJ, Xiong W, Wang X, Min Q, Luo CD, et al. A rat model of oral submucous fibrosis induced by bleomycin. *Oral Surg Oral Med Oral Pathol Oral Radiol* **122**, 216-223 (2016)
29. Nishat R, Kumar H. Collagen fibers in oral submucous fibrosis - A polarizing microscopy study using two special stains. *Indian J Pathol Microbiol* **62**, 537-543 (2019)
30. Anura A, Das D, Pal M, Paul RR, Das S, Chatterjee J. Nanomechanical signatures of oral submucous fibrosis in sub-epithelial connective tissue. *J Mech Behav Biomed Mater* **65**, 705-715 (2017)
31. Matte BF, Kumar A, Placone JK, Zanella VG, Martins MD, Engler AJ, et al. Matrix stiffness mechanically conditions EMT and migratory behavior of oral squamous cell carcinoma. *J Cell Sci* **132**, jcs224360 (2019)
32. Rice AJ, Cortes E, Lachowski D, Cheung BCH, Karim SA, Morton JP, et al. Matrix stiffness induces epithelial-mesenchymal transition and promotes chemoresistance in pancreatic cancer cells.

Oncogenesis **6**, e352 (2017)

33. Xu X, Zhang Y, Wang X, Li S, Tang L. Substrate Stiffness Drives Epithelial to Mesenchymal Transition and Proliferation through the NEAT1-Wnt/beta-Catenin Pathway in Liver Cancer. *Int J Mol Sci* **22**, 12066 (2021)
34. Pastushenko I, Blanpain C. EMT Transition States during Tumor Progression and Metastasis. *Trends Cell Biol* **29**, 212-226 (2019)
35. Yang B, Fu M-F, Tang Z-G. [Rat model with oral submucous fibrosis induced by arecoline and mechanical stimulation]. *Hua xi kou qiang yi xue za zhi = Huaxi kouqiang yixue zazhi = West China journal of stomatology* **37**, 260-264 (2019)
36. Shekatkar M, Kheur S, Sanap A, Undale V, Kharat A, Bhalchim V, et al. A novel approach to develop an animal model for oral submucous fibrosis. *Med Oncol* **39**, 162 (2022)
37. Reshma V, Varsha BK, Rakesh P, Radhika MB, Soumya M, D'Mello S. Aggrandizing oral submucous fibrosis grading using an adjunct special stain: A pilot study. *J Oral Maxillofac Pathol* **20**, 36-46 (2016)
38. Prasad RS, Pai A, Shyamala K, Bhadranna A, Shenoy S, Yaji A. Assessment of epithelial-mesenchymal transition signatures in oral submucous fibrosis. *Journal of oral and maxillofacial pathology : JOMFP* **23**, 308 (2019)
39. Dai J, Qin L, Chen Y, Wang H, Lin G, Li X, et al. Matrix stiffness regulates epithelial-mesenchymal transition via cytoskeletal remodeling and MRTF-A translocation in osteosarcoma cells. *J Mech Behav Biomed Mater* **90**, 226-238 (2019)
40. Gaub BM, Muller DJ. Mechanical Stimulation of Piezo1 Receptors Depends on Extracellular Matrix Proteins and Directionality of Force. *Nano Lett* **17**, 2064-2072 (2017)
41. Chen X, Wanggou S, Bodalia A, Zhu M, Dong W, Fan JJ, et al. A Feedforward Mechanism Mediated by Mechanosensitive Ion Channel PIEZO1 and Tissue Mechanics Promotes Glioma Aggression. *Neuron* **100**, 799-815.e797 (2018)
42. Dupont S, Morsut L, Aragona M, Enzo E, Giulitti S, Cordenonsi M, et al. Role of YAP/TAZ in mechanotransduction. *Nature* **474**, 179-183 (2011)
43. Zanconato F, Forcato M, Battilana G, Azzolin L, Quaranta E, Bodega B, et al. Genome-wide association between YAP/TAZ/TEAD and AP-1 at enhancers drives oncogenic growth. *Nat Cell Biol* **17**, 1218-1227 (2015)
44. Bora-Singhal N, Nguyen J, Schaal C, Perumal D, Singh S, Coppola D, et al. YAP1 Regulates OCT4 Activity and SOX2 Expression to Facilitate Self-Renewal and Vascular Mimicry of Stem-Like Cells. *Stem Cells* **33**, 1705-1718 (2015)
45. Oh SH, Swiderska-Syn M, Jewell ML, Premont RT, Diehl AM. Liver regeneration requires Yap1-TGFbeta-dependent epithelial-mesenchymal transition in hepatocytes. *J Hepatol* **69**, 359-367 (2018)
46. Vincent-Mistiaen Z, Elbediwy A, Vanyai H, Cotton J, Stamp G, Nye E, et al. YAP drives cutaneous squamous cell carcinoma formation and progression. *eLife* **7**, e33304 (2018)

47. Chole RH, Gondivkar SM, Gadbail AR, Balsaraf S, Chaudhary S, Dhore SV, et al. Review of drug treatment of oral submucous fibrosis. *Oral Oncol* **48**, 393-398 (2012)
48. Kerr AR, Warnakulasuriya S, Mighell AJ, Dietrich T, Nasser M, Rimal J, et al. A systematic review of medical interventions for oral submucous fibrosis and future research opportunities. *Oral Dis* **17 Suppl 1**, 42-57 (2011)
49. Angadi PV, Rao S. Management of oral submucous fibrosis: an overview. *Oral Maxillofac Surg* **14**, 133-142 (2010)
50. Atcha H, Jairaman A, Holt JR, Meli VS, Nagalla RR, Veerasubramanian PK, et al. Mechanically activated ion channel Piezo1 modulates macrophage polarization and stiffness sensing. *Nat Commun* **12**, 3256 (2021)
51. Pan W, Wang Q, Zhang Y, Zhang N, Qin J, Li W, et al. Verteporfin can Reverse the Paclitaxel Resistance Induced by YAP Over-Expression in HCT-8/T Cells without Photoactivation through Inhibiting YAP Expression. *Cellular physiology and biochemistry : international journal of experimental cellular physiology, biochemistry, and pharmacology* **39**, 481-490 (2016)
52. Livak KJ, Schmittgen TD. Analysis of relative gene expression data using real-time quantitative PCR and the 2(-Delta Delta C(T)) Method. *Methods (San Diego, Calif)* **25**, 402-408 (2001)

Figures

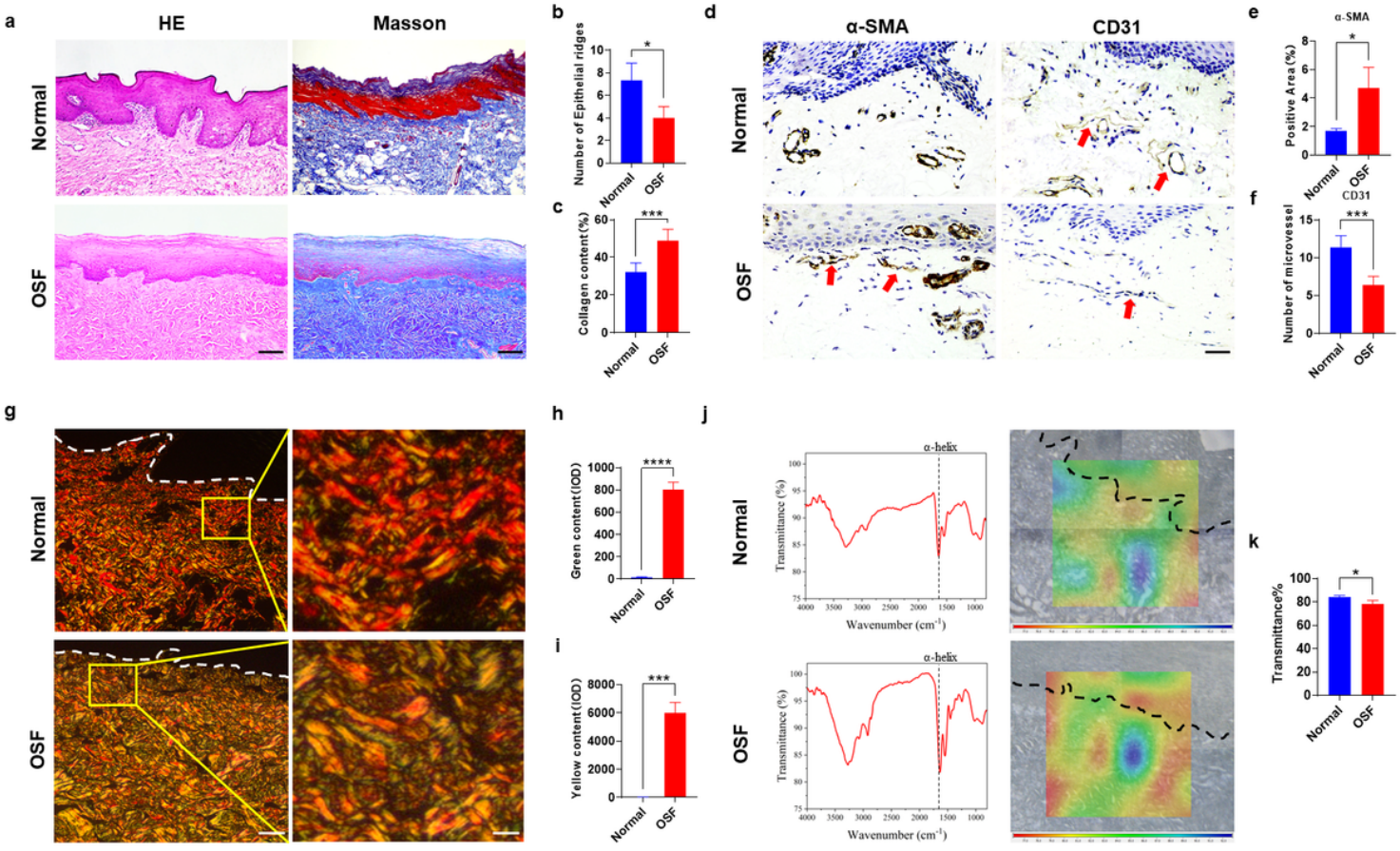

Figure 1

Pathological characteristics of human fibrotic mucosa (n = 6). (**a**) Images of human normal and fibrotic oral mucosa (oral submucous fibrosis (OSF)) stained with hematoxylin and eosin and Masson staining (Scale bar: 200 μm). (**b-c**) According to the results in (**a**), the number of mucosal epithelial processes and the collagen content were analyzed semi-quantitatively. (**d**) Normal and OSF mucosal alpha smooth muscle actin (α-SMA) and CD31 (PECAM1, platelet and endothelial cell adhesion molecule 1) immunohistochemical staining image, red arrows point to myofibroblasts and blood vessel (Scale bar: 50 μm). (**e-f**) Semi-quantitative analysis of the positive areas according to the results in (**d**). (**g**) In Sirius red staining images of normal and OSF mucosa, yellow represents type I and III collagen, and green represents type III collagen (Scale bar: 50 μm, 10 μm). (**h-i**) Semi-quantitative analysis of the yellow and green areas according to the results in (**g**). (**j**) Microscopic infrared analysis images of normal and OSF mucosa. (**k**) Quantitative analysis of the absorption peak according to the results in (**j**). All analysis data represent the mean ± standard deviation determined using one-way analysis of variance (ANOVA) ($p < 0.05$).

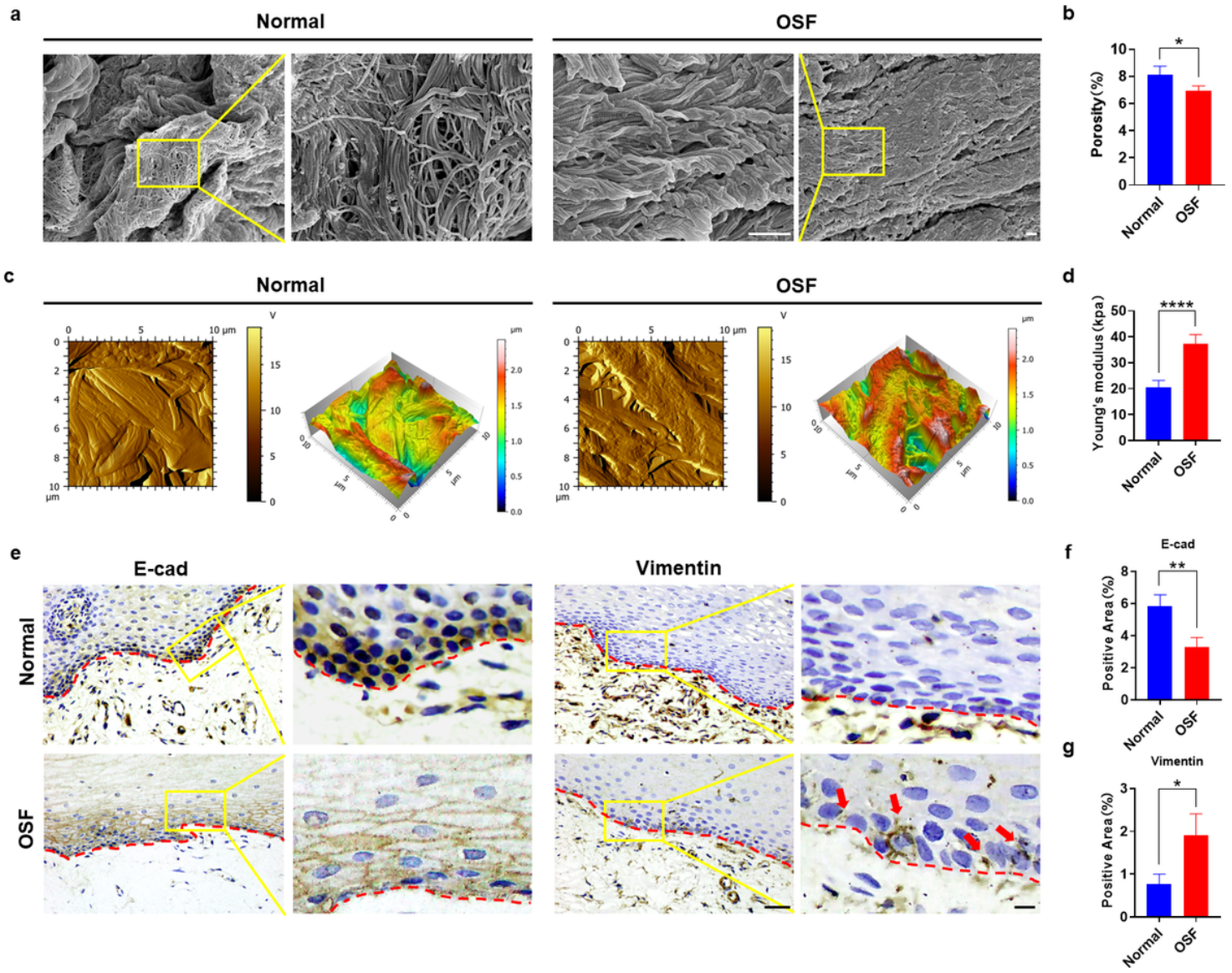

Figure 2

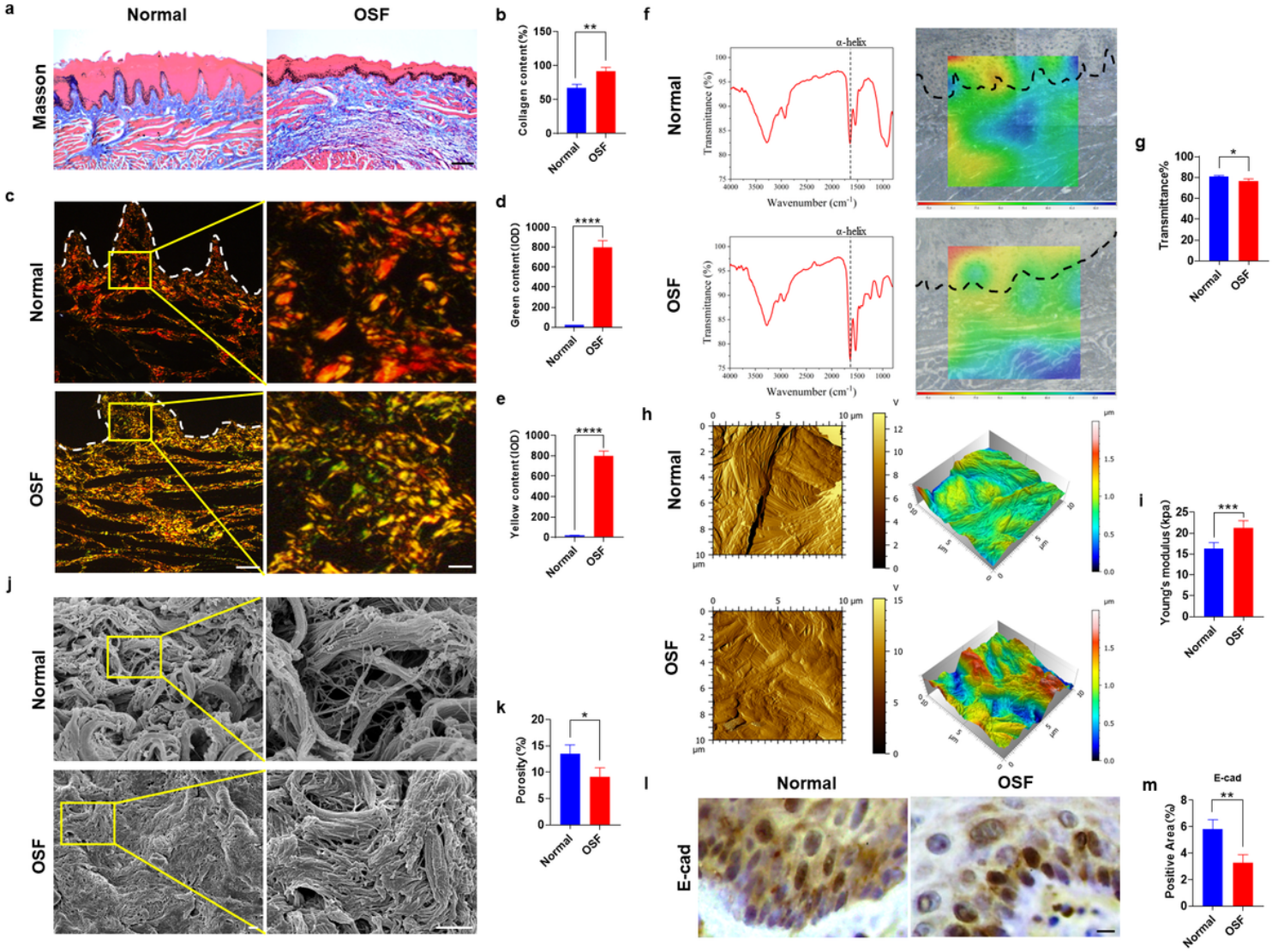

Structural characteristics of human fibrotic mucosa(n = 6). (**a**) Scanning electron microscope image of the oral mucosa lamina propria (Scale bar: 10 μm), (**b**) Quantitative analysis of collagen porosity. (**c**) Atomic force scanning topography image and corresponding three-dimensional reconstruction image of the oral mucosa lamina propria. (**d**) The Young's modulus of the oral mucosa lamina propria analyzed using atomic force microscopy. (**e**) E-cadherin (E-cad) and Vimentin immunohistochemical staining images of the oral mucosal epithelium (Scale bar: 50 μm, 10 μm). **(f-g)** Semi quantitative analysis on the positive area according to the results in (**e**). All analysis data represent the mean ± standard deviation determined using one-way analysis of variance (ANOVA) ($p < 0.05$).

Figure 3

Characteristics of fibrotic oral mucosa in rats(n = 6). (**a**) Images of normal and oral submucous fibrosis (OSF) mucosa stained using Masson staining (Scale bar: 200 μm). (**b**) The collagen content of the mucosa analyzed-semi quantitatively. (**c**) Sirius red staining image of normal and OSF mucosa (Scale

bar: 50 μm, 10μm). (**d-e**) Semi quantitative analysis of the yellow and green areas according to the results in (**c**). (**f**) Microscopic infrared analysis images of normal and OSF mucosa. (**g**) Quantitative analysis of the absorption peak according to the results in (**f**). (**h**) Atomic force scanning topographic map of the oral mucosa lamina propria and corresponding three-dimensional reconstruction image. (**i**) The Young's modulus of the oral mucosa lamina propria analyzed using atomic force microscopy. (**j**) Scanning electron microscope image of the oral mucosa lamina propria (Scale bar: 10 μm), (**k**) Quantitative analysis of collagen porosity. (**l**) E-cadherin (E-cad) immunohistochemical staining image of the oral mucosa epithelium (Scale bar: 10 μm). (**m**) Semi-quantitative analysis of the positive areas was performed according to the results in (**l**). All analysis data represent the mean ± standard deviation determined using one-way analysis of variance (ANOVA) ($p < 0.05$).

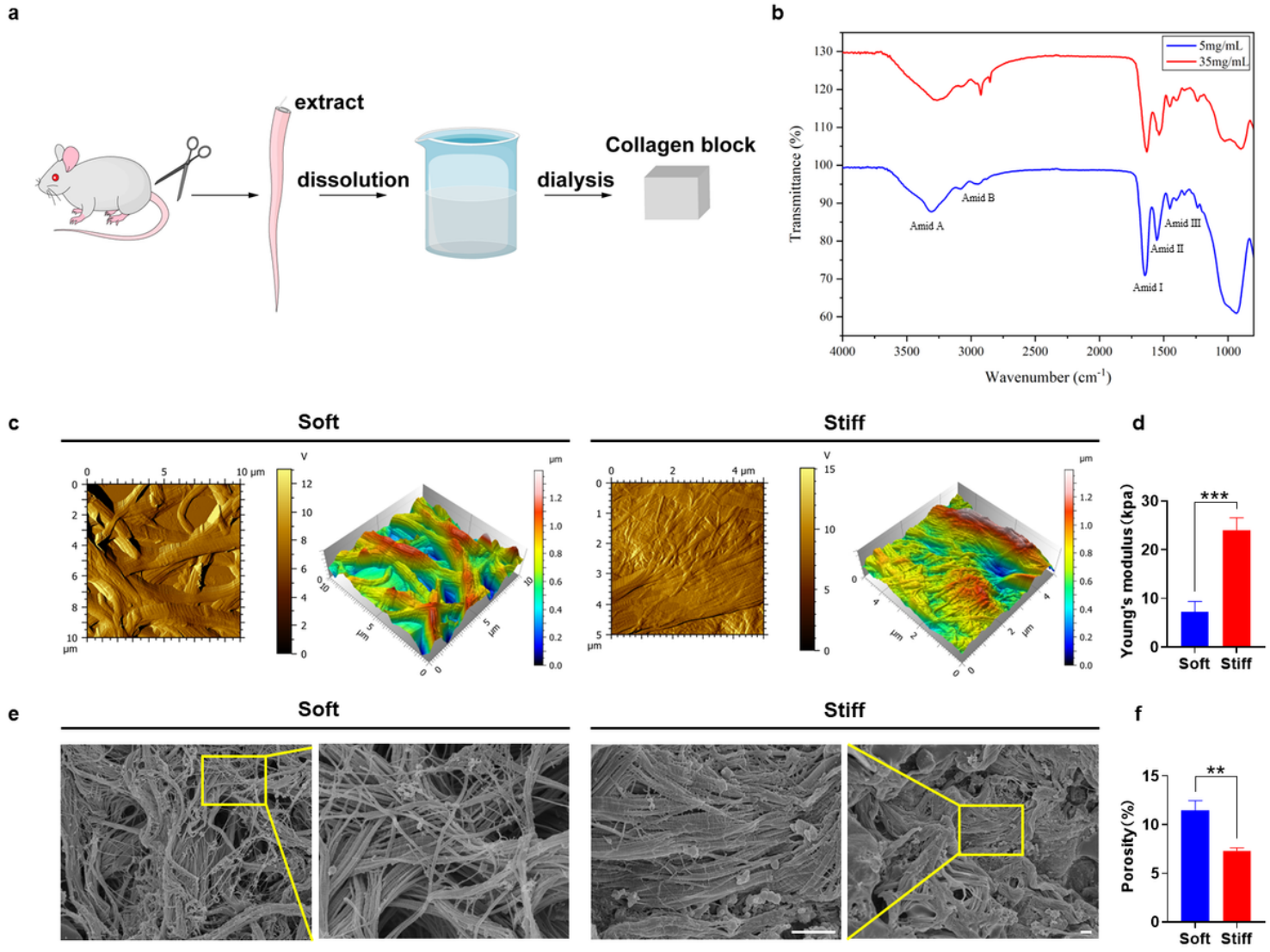

Figure 4

Construction and characterization of collagen constructs (n = 6). (**a**) Schematic diagram of collagen gel matrix construction. (**b**) Infrared spectrum of collagen gel. (**c**) Atomic force scanning topographic map of collagen gel matrix and corresponding three-dimensional reconstruction image. (**d**) The Young's modulus

of the collagen matrix analyzed using atomic force microscope. (**e**) Scanning electron microscope image of the collagen gel (Scale bar: 10 μm). (**f**) Quantitative analysis of collagen gel porosity. All analysis data represent the mean ± standard deviation determined using one-way analysis of variance (ANOVA) ($p < 0.05$).

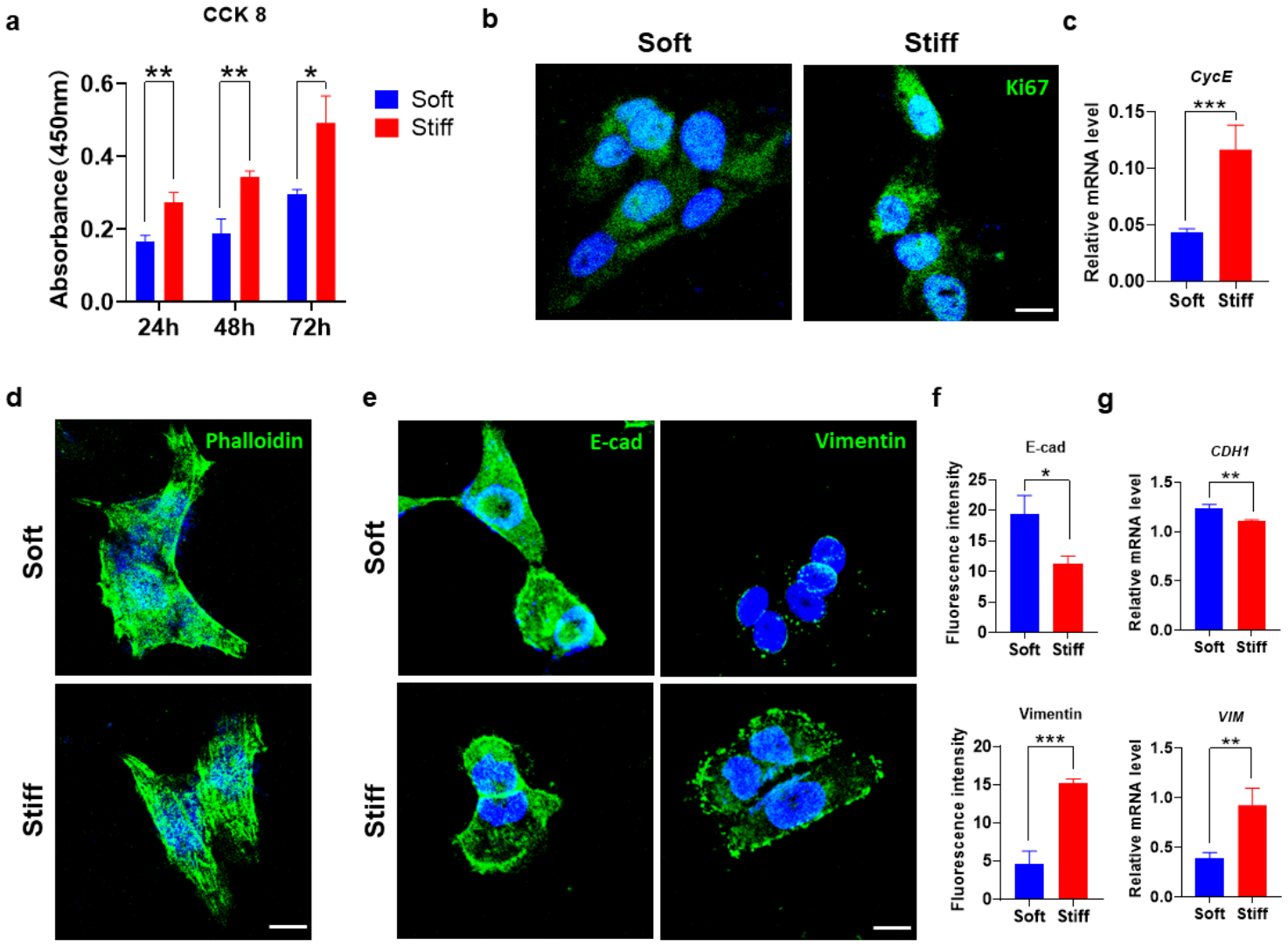

Figure 5

Stiff matrix promotes mesenchymal transformation of epithelial cells (n = 6). (**a**) The proliferation of cells cultured on different stiff matrices for 24, 48 and 72 hours. (**b**) Representative images of Ki67 immunostaining (Scale bar: 10 μm). (**c**) The expression of cyclin E in cells cultured on different stiff matrices for 24 hours. (**d**) Representative images of cytoskeleton immunostaining after 24 hours of culture on different stiff matrices (Scale bar: 10 μm). (**e**) Representative images of E-cadherin (E-cad) and vimentin immunostaining in cells cultured on different stiff matrices for 24 hours (Scale bar: 10 μm). (**f**) Semi quantitative analysis of fluorescence intensity is performed according to the results in (**e**). (**g**) The expression of CDH1 and VIM genes in cells cultured on different stiff matrices for 24 hours. All analysis

data represent the mean ± standard deviation determined using one-way analysis of variance (ANOVA) ($p < 0.05$).

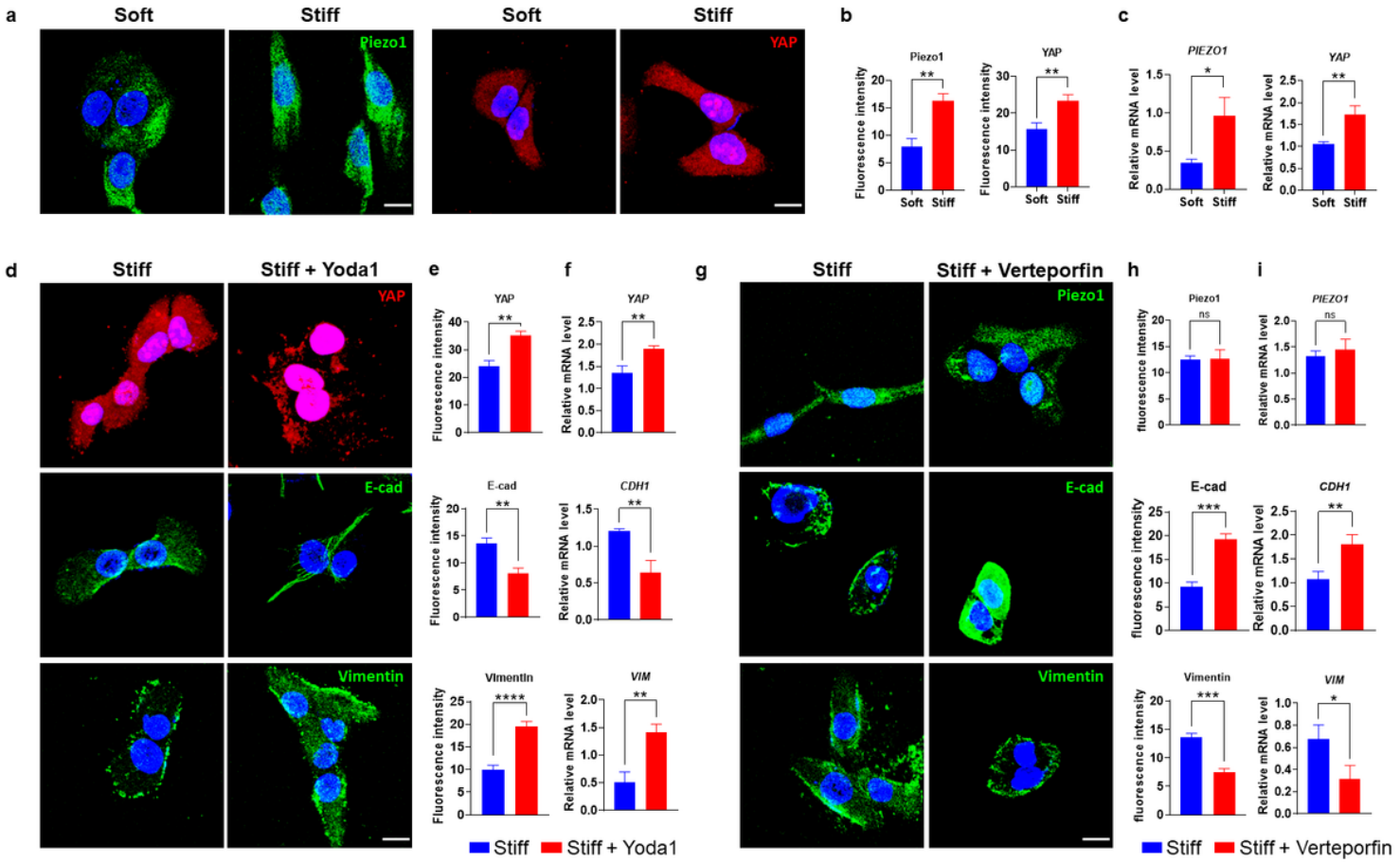

Figure 6

Piezo1 and YAP mediated mesenchymal transformation of epithelial cells (n = 6). (**a**) Representative images of immune staining of piezo type mechanosensitive ion channel component 1 (Piezo1) and yes-associated protein (YAP) in cells cultured on different stiff matrices for 24 hours (Scale bar: 10 μm). (**b**) Semi-quantitative analysis of the fluorescence intensity according to the results in (**a**). (**c**) Levels of Piezo1 and YAP in cells cultured on different stiff matrices for 24 hours. (**d**) The representative images of YAP, E-cadherin (E-cad), and vimentin immunostaining in cells cultured on stiff matrices for 24 hours with or without Yoda1 ((2-[5-[[(2,6-Dichlorophenyl)methyl]thio]-1,3,4-thiadiazol-2-yl]-pyrazine) (Scale bar: 10 μm). (**e**) Semi-quantitative analysis of the fluorescence intensity according to the results in (**d**). (**f**) Expression of the *YAP*, *CDH1* (E-cad), and *VIM* (vimentin) genes in cells cultured on stiff matrices for 24 hours, with or without Yoda1. (**g**) Representative images of Piezo1, E-cad, and vimentin immunostaining in cells cultured on stiff matrices for 24 hours, with or without Verteporfin. (Scale bar: 10 μm). (**h**) Semi-quantitative analysis of the fluorescence intensity according to the results in (**g**). (**i**) Expression of the *PIEZO1*, *CDH1*, and *VIM* genes in cells cultured on stiff matrices for 24 hours, with or without Verteporfin. All analysis data represent the mean ± standard deviation determined using one-way analysis of variance (ANOVA) ($p < 0.05$).

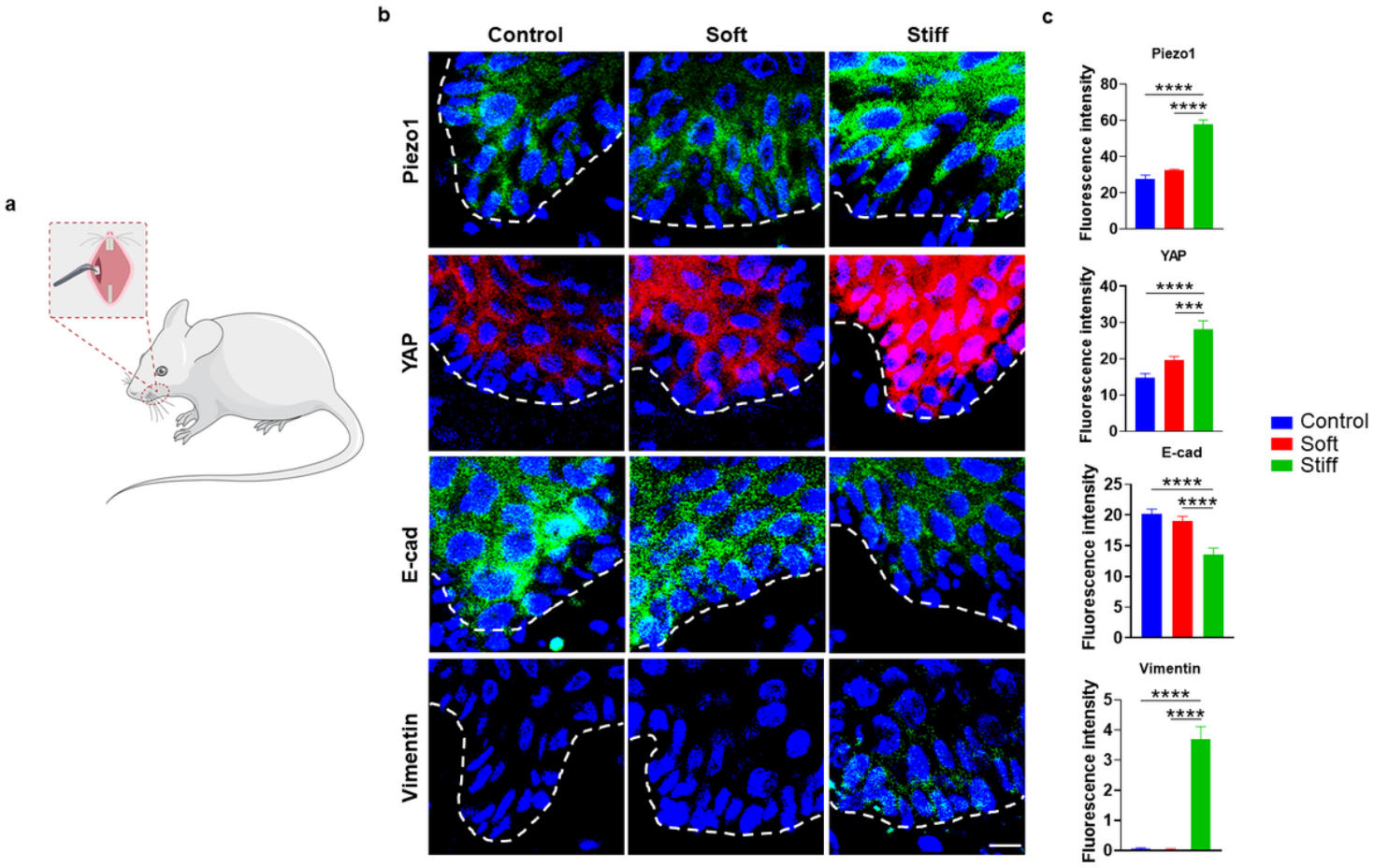

Figure 7

Stiff collagen matrix promotes mesenchymal transformation of rat epithelial cells (n = 6). (**a**) Schematic diagram of subcutaneous collagen implantation in rats. (**b**) Representative images of piezo type mechanosensitive ion channel component 1 (Piezo1), yes-associated protein (YAP), E-cadherin (E-cad), and vimentin immunostaining in rat oral mucosal epithelium after implantation of collagen (Scale bar: 50 μm). (**c**) Semi-quantitative analysis of the fluorescence intensity according to the results in (**b**). All analysis data represent the mean ± standard deviation determined using one-way analysis of variance (ANOVA) ($p < 0.05$).

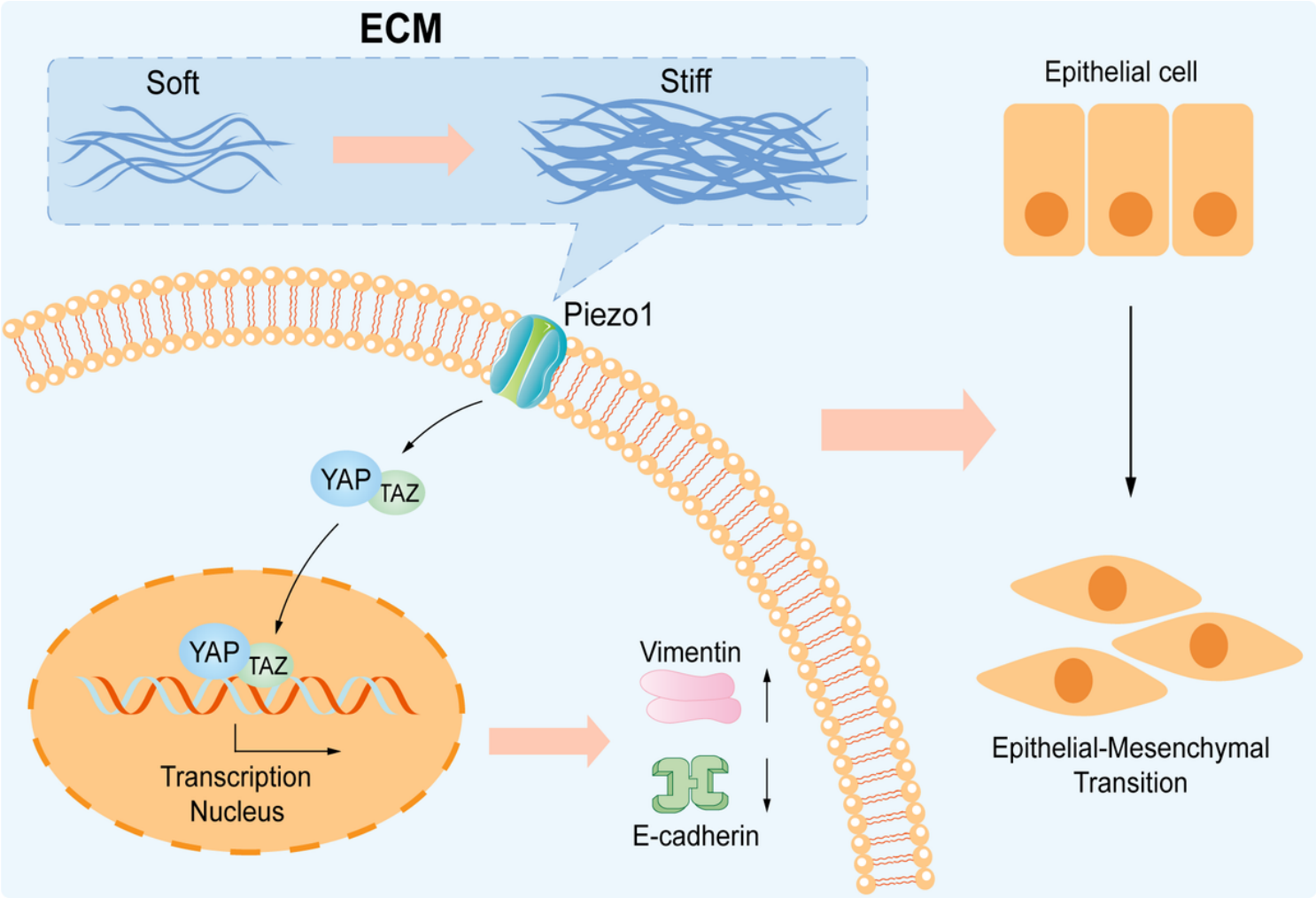

Figure 8

Diagram of the mechanism by which matrix stiffness induces mesenchymal transformation of epithelial cells. Cells sense the mechanical changes of the extracellular matrix (ECM) through piezo type mechanosensitive ion channel component 1 (Piezo1). In the presence of exogenous transforming growth factor beta (TGF-β), when the stiffness of ECM increases, the expression of Piezo1 increases and the ion channel opens, its downstream yes-associated protein (YAP) will undergo nuclear translocation, which will affect the expression of EMT-related proteins E-cadherin (E-cad) and vimentin in cells, thus causing cells to undergo epithelial mesenchyme transition (EMT).

Supplementary Files

This is a list of supplementary files associated with this preprint. Click to download.

- Supplementary.docx